RGO-CoO-$Ni(OH)_2$ as an electrode material of supercapacitor

P.Y. Chan and S.R. Majid*

Centre for Ionics University of Malaya, Department of Physics, Faculty of Science, University of Malaya, 50603 Kuala Lumpur, Malaysia.

Corresponding author*: Tel: +60379674146/4238

E-mail address: shana@um.edu.my

Abstract

A composite film containing reduced graphene oxide (RGO), CoO and $Ni(OH)_2$ has been prepared from $Co(NO_3)_2.6H_2O$ and $Ni(NO_3)_2.6H_2O$ with its Co:Ni ratio of 2:1 using simple electrodeposition technique. The effect of scan rate on the electrode film is highlighted. Changes in cyclic voltammetry (CV) curves and thus morphologies of the electrode film after CV test are identified. The electrode film exhibits specific capacitance of 558 $F\ g^{-1}$ at 5 $mV\ s^{-1}$ in 1M KOH. However, the cycling stability of the electrode film over 1000 cycles is low and need to be improved further. The morphology of the electrode film is demonstrated using field emission scanning electron microsope (FESEM).

Keywords: reduced graphene oxide, CoO, $Ni(OH)_2$, cyclic voltammetry

1.0 Introduction

Electrochemical capacitor (EC), also called supercapacitor is well known for its high power capability and long cycle life as an energy storage device [1]. It can be used complementary with battery to achieve better performance for a device. In general, there are two basic types of supercapacitor: one is electrochemical double layer capacitor (EDLC) that utilizes the high surface area of carbon materials to store charge based on electrostatic reaction, another one is the pseudocapacitor that relies on the capacitance contributed by the redox reactions offered by the transition metal oxides and conducting polymers. EDLC has low energy density due to the charge storage is actually simply based on adsorption/desorption process. Pseudocapacitor always can achieve higher specific capacitance due to the storage mechanism that is not limited to physical interactions but determined by the electron transfer processes occured at interface of electrode/electrolyte. An electrode is where the reactions occurred and used to store charge. In order to produce high performance of supercapacitor, it is very important to synthesize the electrode material with suitable microstructure that can offer a good pathway for electron transfers inside electrode and insertion/deinsertion processes of electrolyte ions on electrode surface.

Transition metal oxides/hydroxides (e.g. RuO_2, MnO_2, CoO, $Ni(OH)_2$, NiO, ZnO) are studied widely due to their multiple oxidation states that offer redox reactions and high theoretical specific capacitance [2-7]. However, due to the poor conductivity nature, there is only part of the active materials taking part in the electron transportations. Many works have been carried out underway to investigate the preparation methods in order to enhance the electrochemical

utilization of transition metal oxide/hydroxide. The combination of two metal oxides/hydroxides or so called binary metal oxides/hydroxides based electrode is believed to behave better than one metal oxide based electrode. $Ni(OH)_2$ is well known for its low cost and very flexible in forming desirable morphology based on different preparation methods [8-11]. On the other hand, cobalt based oxides such as CoO and Co_3O_4 are attractive electrode candidates due to their high electroactivity and good electrochemical performances [12-14].

There are some reports about the electrochemical performances of the $Ni(OH)_2$ based or Co based oxides electrodes [8-14]. There are also studies regarding to the combination of these two materials using different preparation methods [15, 16]. Herein, we report a simple electrodeposition technique to fabricate the composite directly on a stainless steel. It is known that the performance of the electrode material strongly depends on the particle properties for example crystallinity, structure and particle size. All this determines by the synthetic method applied. Electrodeposition technique offers certain advantages for the fabrication of electrode film, for example thin film with specific structure and chemical properties can be prepared. The physical properties can be controlled by means of electrodeposition variables such as the electrolyte composition, electrolyte concentration, applied potential, applied current density and electrodeposition duration. Besides, by deposited transition metal oxide on electronically conductive substrate such as stainless steel allow us to study the fundamental electrochemical behaviour of the film formed. In our work, we applied chronopotentiometry method for the electrodeposition of the composite with reduced graphene oxide. The morphology and electrochemical performance of the electrode film produced were examined.

2.0 Methodology

2.1 Materials

Sulfuric acid (H_2SO_4), phosphoric acid (H_3PO_4), hydrogen peroxide 30% (H_2O_2), hydrogen chloride (HCl) (Friendemann Schmidt), graphite flakes (Nippon Graphite Industries, Ltd), potassium permanganate ($KMnO_4$) (Bendosen), L-ascorbic acid (UNILAB), nickel (II) nitrate hexahydrate ($Ni(NO_3)_2.6H_2O$) (Unilab), cobalt (II) nitrate hexahydrate ($Co(NO_3)_2.6H_2O$) (Sigma Aldrich) and sodium acetate (CH_3COONa) (Univar) were used as received.

2.2 Preparation and characterizations of RGO-CoO-$Ni(OH)_2$ based electrode film

Chronopotentiometry deposition technique was applied in this study. The current density used for deposition was -2mA cm^{-2}. RGO was prepared firstly as shown in our previous study [17]. RGO was mixed with 8mmol $Co(NO_3)_2.6H_2O$, 4mmol $Ni(NO_3)_2.6H_2O$ and 0.1M CH_3COONa. This solution was stirred without heat overnight and being served as electrolyte for electrodeposition. Since the potential was not fixed in this technique, two-electrode configuration was used at where (2x2) cm^2 stainless steel and carbon rod acting as working and counter electrode respectively. After electrodeposition for 10 minutes, the deposited stainless steel was rinsed with distilled water and heated at 100°C for 3 hours. The deposited film was then ready for characterizations.

The weights of bare and deposited stainless steels were measured using a high precision microbalance (Mettler Toledo MT5). The weight of the composite film was estimated by subtracting the weight of the bare stainless steel by the weight of the deposited stainless steel.

All electrochemical measurements were carried out in a three-electrode setup in 1M KOH at room temperature: deposited stainless steel served as the working electrode, a platinum electrode and an Ag/AgCl electrode served as counter and reference electrode respectively. AUT50029 was used to measure the electrochemical performances: cyclic voltammetry (CV), galvanostatic charge-discharge (CD) and frequency response analysis (FRA). CV tests were performed between -0.2 and 0.4 V (vs. Ag/AgCl) at different scan rates of 1, 5, 10, 15 and 20 mV s^{-1}. CD measurements were done in the potential range of 0.0 to 0.4 V at different current densities of 1, 5, 10, 15 and 20 A g^{-1}. FRA was carried out in the frequency range from 100 kHz to 0.1 Hz. The specific capacitance can be obtained from CV curve and calculated according to equation below:

$$C_{sp} = (\int I\, dV) / (\nu.m.V) \text{ ----- (1)}$$

at where I = response current density , ν=scan rate, m = weight of the composite film and V = potential.

The morphology and microstructure of the electrode film were studied using Jeol JSM-7600F field emission scanning electron microscopy (FESEM) and Jeol JEM-2100F transmission electron microscopy (TEM) respectively. The elements presented in the composite film were investigated using energy-dispersive X-ray spectroscopy (EDX). The nature of the composite film was analyzed using D8-advance X-ray diffraction XRD Bruker AXS with CuK_{α} monochromatized radiation at 40kV and 40mA at ambient temperature.

3.0 Results and Discussions:

3.1 X-ray diffraction (XRD) and Energy-dispersive X-ray spectroscopy (EDX)

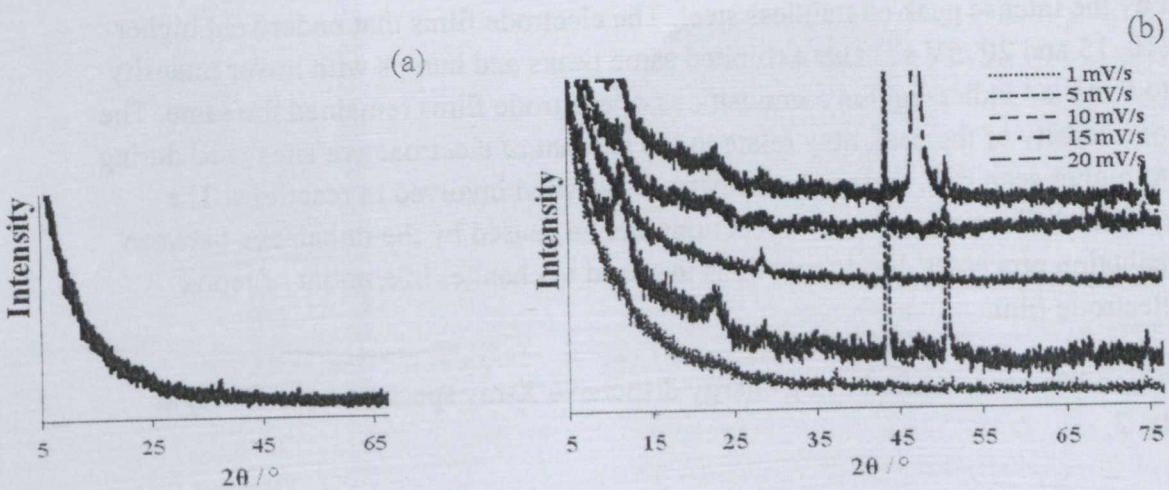

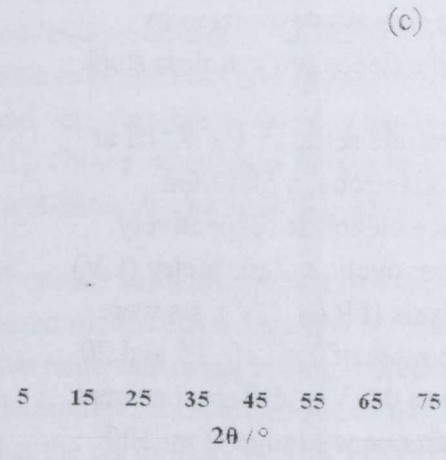

Figure 1: XRD pattern of (a) as-prepared electrode film (powder), (b) electrode films on stainless steel after different scan rates and (c) bare stainless steel

Fig. 1(a) shows the XRD patterns of the as-prepared electrode film scrapping of from the stainless steel. No obvious peaks were found indicating the structure formed is amorphous in nature. However, there were structural changes detected after the cyclic voltammetry tests implying that the irreversibity of the electrode films.

Fig. 1(b) displays the XRD patterns of electrode films after experienced different scan rates. As shown, the electrode film exhibited no diffraction peaks at 1 mV s^{-1} showing well depositing film on the stainless steel at where the diffraction peaks of stainless steels were not detected. Two obvious sharp peaks, two broad humps and one small hump were recognised for electrode film experienced 5 mV s^{-1}. By comparing to Fig. (c), the sharp peaks can be attributed to the stainless steel, which is exposed after reactions. The broad humps at at around 12° and 23° can be attributed to (001) and (006) planes of α-$Ni(OH)_2$ [18]. The small hump at around 74° can be assigned to (311) planes of CoO. In fact, CoO has a diffraction peak located around 44° belonged to (200) plane (JCPDS 75-0393). However, it may overlapped by the intense peak of stainless steel. The electrode films that underwent higher scan rates (10, 15 and 20 mV s^{-1}) also exhibited same peaks and humps with lower intensity compared to 5 mV s^{-1} indicating the compositions of electrode films remained the same. The difference of intensity of the peak may relate to the amount of electroactive sites used during reactions. At higher scan rate, there is less electroactive sited involved in reactions. The appearance of the diffraction peaks after reactions can be caused by the imbalance between oxidation/reduction processes during reactions that lead to changes in amount of redox species in electrode film.

The composition has been verified using energy dispersive X-ray spectroscopy (EDX) as shown in Fig. 2.

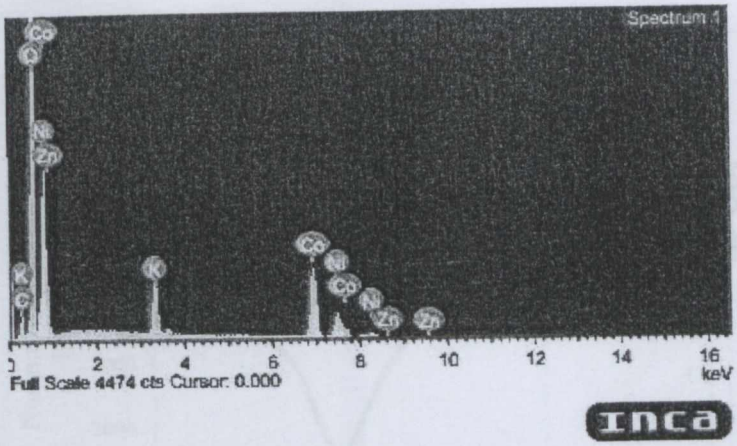

Fig. 2: EDX spectra of electrode film undergo 5 mV s^{-1}.

Fig. 2 displays the elements present inside the electrode film after 5 mV s^{-1}. There are Co, Ni, C and K which is consistent to the XRD and TEM lattice fringes results. The appearance of K on the electrode film indicates that the there is some insertions of electrolyte ions during the cyclic voltammetry test.

3.2 Electrochemical tests

The electrochemical performance of RGO-CoO-$Ni(OH)_2$ composite electrode can be tested using cyclic voltammetry (CV), galvanostatic charge-discharge (CD) and frequency response analysis (FRA) in three-electrode configuration.

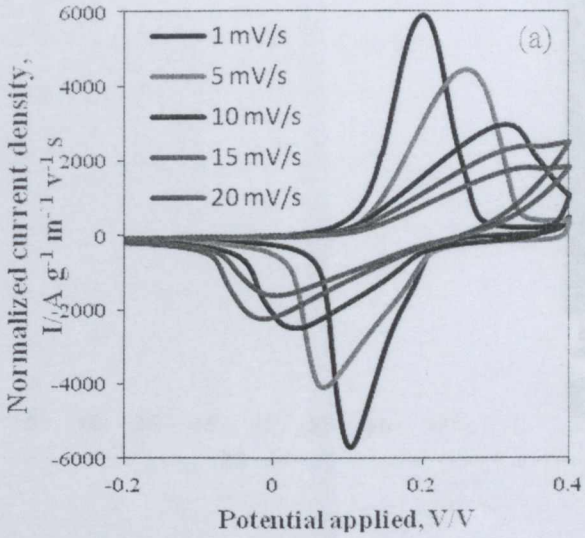
(a)
1 mV/s
5 mV/s
10 mV/s
15 mV/s
20 mV/s
Normalized current density, I/A g⁻¹ m⁻¹ V⁻¹ s
Potential applied, V/V

(b)

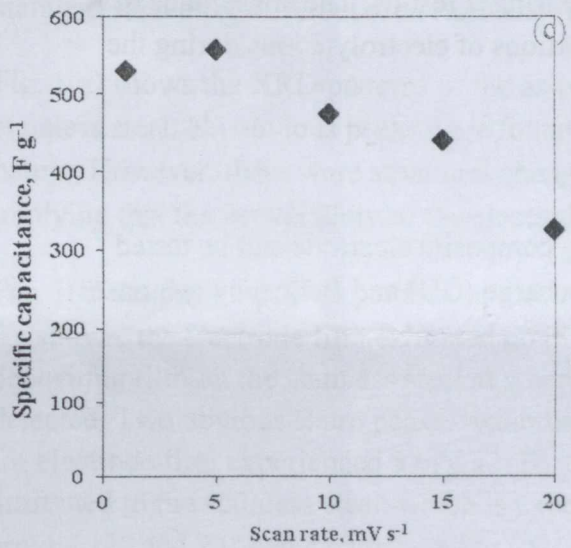
(c)
Specific capacitance, F g⁻¹
Scan rate, mV s⁻¹

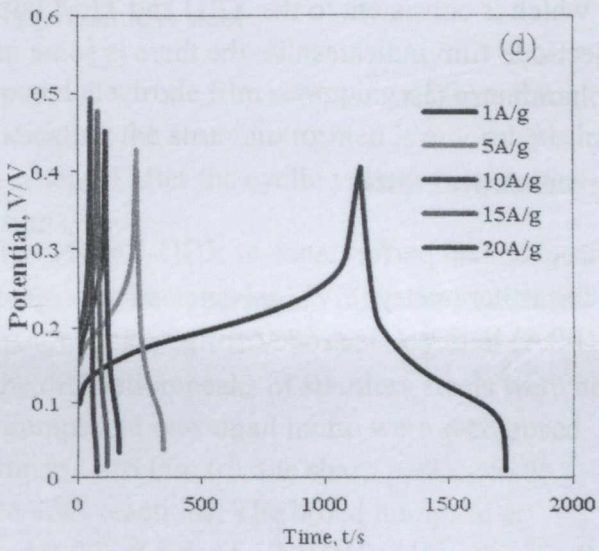
(d)
1A/g
5A/g
10A/g
15A/g
20A/g
Potential, V/V
Time, t/s

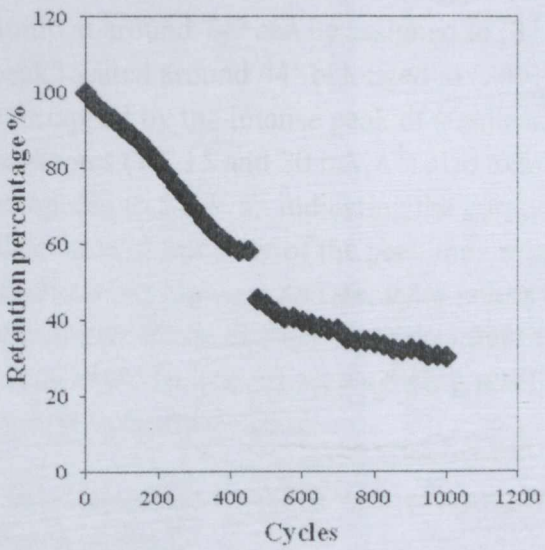
Retention percentage %
Cycles

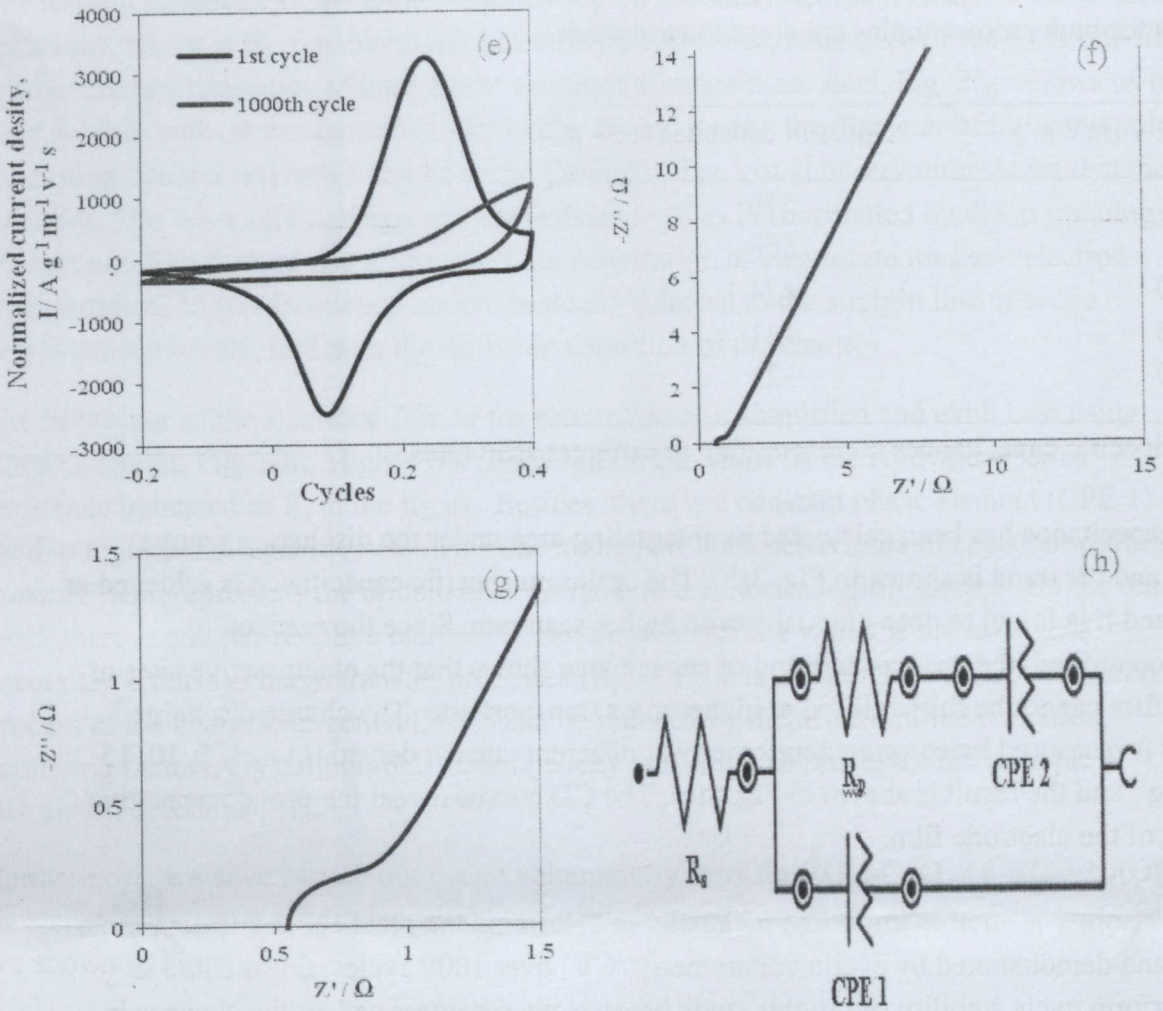

Figure 3: RCN10mins (a) normalized CV curves with different scan rates, (b) specific capacitance vs scan rate, (c) galvanostatic charge-discharge curves at different current density, (d) capacitance retention test, (e) CV curves before and after 1000 cycles, (f,g) Nyquist plot of electrode film before electrochemical test and (h) equivalent circuit for electrode film.

Cyclic voltammetry (CV) is a versatile electroanalytical technique used to study the electrochemical reactions. It can be used to determine the redox potentials and identify the redox species. Fig. 3(a) shows the effect of scan rate on the CV curves of the electrode film in 1M KOH. The scan rates are 1, 5, 10, 15 and 20 mV s^{-1}. For more clarity, peak currents were normalized with scan rate and presented in Fig. 3(a). Generally, a pair of well defined redox peaks can be observed in all CV curves within -0.2 V to 0.4 V. The redox peaks become broader with higher scan rate. Besides, the oxidation and reduction peaks shift to more positive and more negative potential respectively when the scan rate increases. The changes of redox potential and peak current density indicate the redox peaks were scan rate dependent and the electron transfer rate is slow. The electrode film may experience chemical change which is due to the insertion of electrolyte ions inside the film. The morphology after electrochemical test has been carried out using field emission scanning electron microscope (FESEM). During 1 mV s^{-1}, the anodic and cathodic peaks at around 0.2V and 0.18V can be assigned to transition reactions of Co(II)/Co(III) and Ni(II)/Ni(III) redox couples [19]. There

is only one set of redox peaks being detected. This is due to the reason that the redox potentials for both redox couples are close to each other.

Scan rate, ν (mV s^{-1})	Specific capacitance (F g^{-1})
1	530
5	558
10	474
15	441
20	325

Table 1: Specific capacitances corresponding to different scan rates.

Specific capacitance has been calculated by integrating area under the discharging curve (Table 1) and the trend is shown in Fig. 3(b). The optimum specific capacitance is achieved at 5 mV s^{-1} and it is found to drop gradually with higher scan rate. Since the reaction is diffusion controlled, the decreasing trend of capacitance shows that the electroactive sites of electrode film cannot be fully utilised at higher mass transport rate. The charge discharge behaviour is measured by chronopotentiometry at different current densities i.e. 1, 5, 10, 15 and 20 A g^{-1} and the result is shown in Fig. 3(c). The CD curves reveal the pseudocapacitive behaviour of the electrode film.

The cycle stability is another important parameter to determine the practical application of an electrode and demonstrated by cyclic voltammetry (CV) over 1000 cycles. CV method is used to perform cycle stability test in this study because we are interested on the changes in reactions of the electrode film after experienced long cycling. The capacitances after every 25 cycles are calculated and the retention percentage of capacitance compared to the initial capacitance is estimated. The capacitance retention test result is shown in Fig. 3(d). As shown, the retention percentage dropped gradually with increasing cycle number until 450th cycle and decreased rapidly after that. This suggests that the cycling stability of the electrode film is low. The CV curves before and after the tests are displayed in Fig. 3(e). The deviation of the curve from the initial CV curve after 1000 cycles is obvious. The redox peaks were disappeared indicating the degradation of the electrode film. The degradation can be caused by (a) the change in active masses volume induced by the difference in volumetric density between oxidized and reduced redox species which leads to the poor electron transportation, and (b) partial dissolution of electrode film after long cycling [20]. Besides, the irreversible chemically change of electrode film during cycling process may also cause the degradation of the electrode film.

The fundamental behaviour of the electrode film has been examined using Frequency Response Analysis (FRA). Fig. 3(f) and (g) exhibits the Nyquist plot of the electrode film performed at the frequency range of 0.1Hz to 0.1MHz in 1M KOH and the equivalent circuit used to fit the data is shown in Fig. 3(h). The Nyquist plot consists of a high frequency intercept on the real axis, a semicircle and a linear region at low frequency range.

The leading resistance in the high frequency region (546mΩ) represents the equivalent series resistance, which is the combination of electrolyte resistance, resistance of the electrode film and the contact resistance of interface at electrode film/stainless steel. Fig. 3(g) allows us to have a detail look on the depressed semicircle. By evaluating the diameter of the semicircle, the charge transfer resistance can be found (368mΩ). The visual observation shows that the electrode film has a small charge transfer resistance. This is contributed by the morphology of electrode film formed that allows the ease penetration of electrolyte ions and electron transportation. Lower frequency region, basically referred to the straight line after the depressed semicircle, indicates the diffusion condition of the charges.

The behaviour of the electrode film in the electrolyte was simplified and explained using Randles circuit, Fig. 3(h). Higher frequency region can show us the equivalent series resistance indicated as R_s in the figure. Besides, there is a constant phase element (CPE 1) used to replace the capacitive elements due to the non-ideal behaviours of capacitor during measurement, represents the double layer formed on the electrode film surface. On the other hand, there is another resistive element in parallel with CPE 1 which is the resistance encountered during charge transfer processes (R_p). CPE 2 is used to describe the diffusion process of the charges. In general, CPE can be induced by diffusion-limited condition, geometric factors, crystallographic heterogeneity and sluggish processes for example adsorption of anions [21].

Furthermore, we have carried out cyclic voltammetry tests for RGO-CoO and RGO-$Ni(OH)_2$ by applying the same electrodeposition and measurement conditions. The CV curves obtained are shown in Fig. 4.

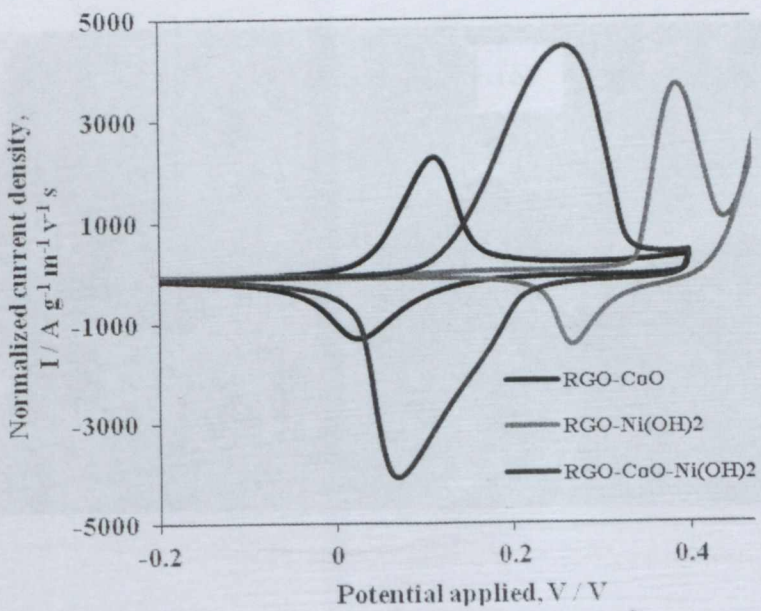

Figure 4: Cyclic voltammetry (CV) curves for RGO-CoO, RGO-$Ni(OH)_2$ and RGO-CoO-$Ni(OH)_2$ at 5 mV s^{-1} in 1M KOH.

The redox peaks appeared in CV curves of RGO-CoO and RGO-$Ni(OH)_2$ can be assigned to the transition reactions between redox couple of Co(II)/Co(III) and Ni(II)/Ni(III) respectively. The plausible reactions are shown as following [22]:

$$CoO + OH^- \leftrightarrow CoOOH + e^-$$

$$Ni(OH)_2 + OH^- \leftrightarrow NiOOH + e^-$$

As seen, the conversion of Ni(II) to Ni(III) occurs right before oxygen evolution. The reduction peak of Ni(III) to Ni(II) is small compared to oxidation peaks of Ni(II) to Ni(III). This shows the irreversibility of Ni(III) and can causes the degradation of electrode film during long cycling. The CV curve of RGO-CoO-$Ni(OH)_2$ presents the redox potentials in between the two potentials of Co and Ni redox species. The current density increases after these two redox species mixed together. As expected, the specific capacitances of individual RGO-CoO and RGO-$Ni(OH)_2$ are lower compared to RGO-(Ni-Co)OH, which are 197 F g^{-1} and 155 F g^{-1} respectively.

3.2 FESEM study

The formation of RGO-CoO-$Ni(OH)_2$ composite film is explained as follows. Firstly, the electro-reduction of nitrate ion produces NO_2^- which further reduce to N_2 and produced OH^-. These hydroxide ions attract Ni and Co cations and form $Ni(OH)_2$ and $Co(OH)_2$ accordingly. The electrochemical reactions can be presented as following [23]:

$$NO_3^- + H_2O + 2e^- \rightarrow NO_2^- + 2OH^-$$

$$2NO_2^- + 4H_2O + 6e^- \rightarrow N_2 + 8OH^-$$

$$Ni^{2+} + 2OH^- \rightarrow Ni(OH)_2$$

$$Co^{2+} + 2OH^- \rightarrow Co(OH)_2$$

The composite film formed is annealed at 100°C for 3 hours which converts the $Co(OH)_2$ to CoO but retain the $Ni(OH)_2$. In order to examine the morphology formed, field emission scanning electron microscopy (FESEM) has been carried out and the images obtained are shown in following.

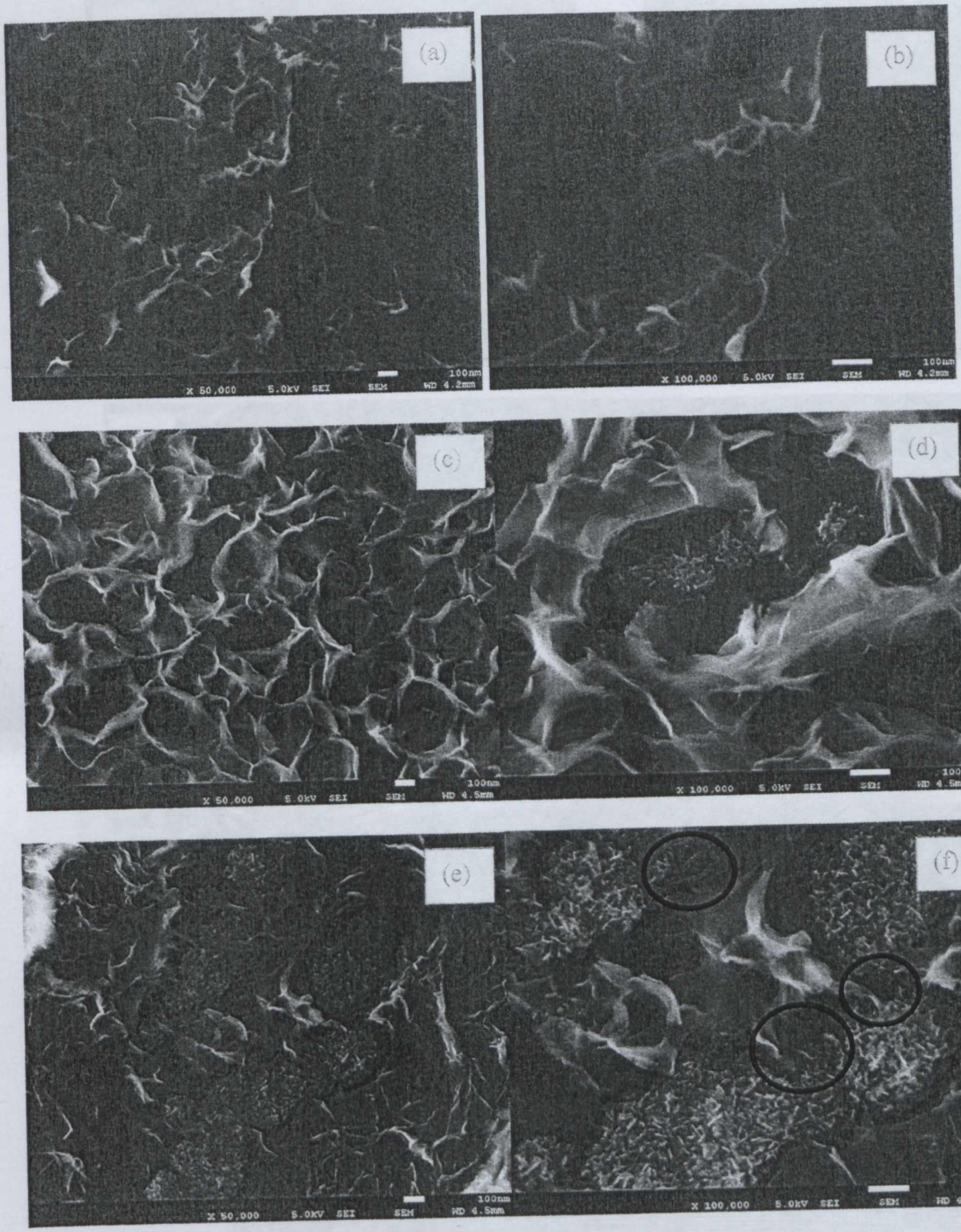
(a)
X 50,000 5.0kV SEI SEM WD 4.2mm 100nm
(b)
X 100,000 5.0kV SEI SEM WD 4.2mm 100nm
(c)
X 50,000 5.0kV SEI SEM WD 4.5mm 100nm
(d)
X 100,000 5.0kV SEI SEM WD 4.5mm 100nm
(e)
X 50,000 5.0kV SEI SEM WD 4.5mm 100nm
(f)
X 100,000 5.0kV SEI SEM WD 4.5mm 100nm

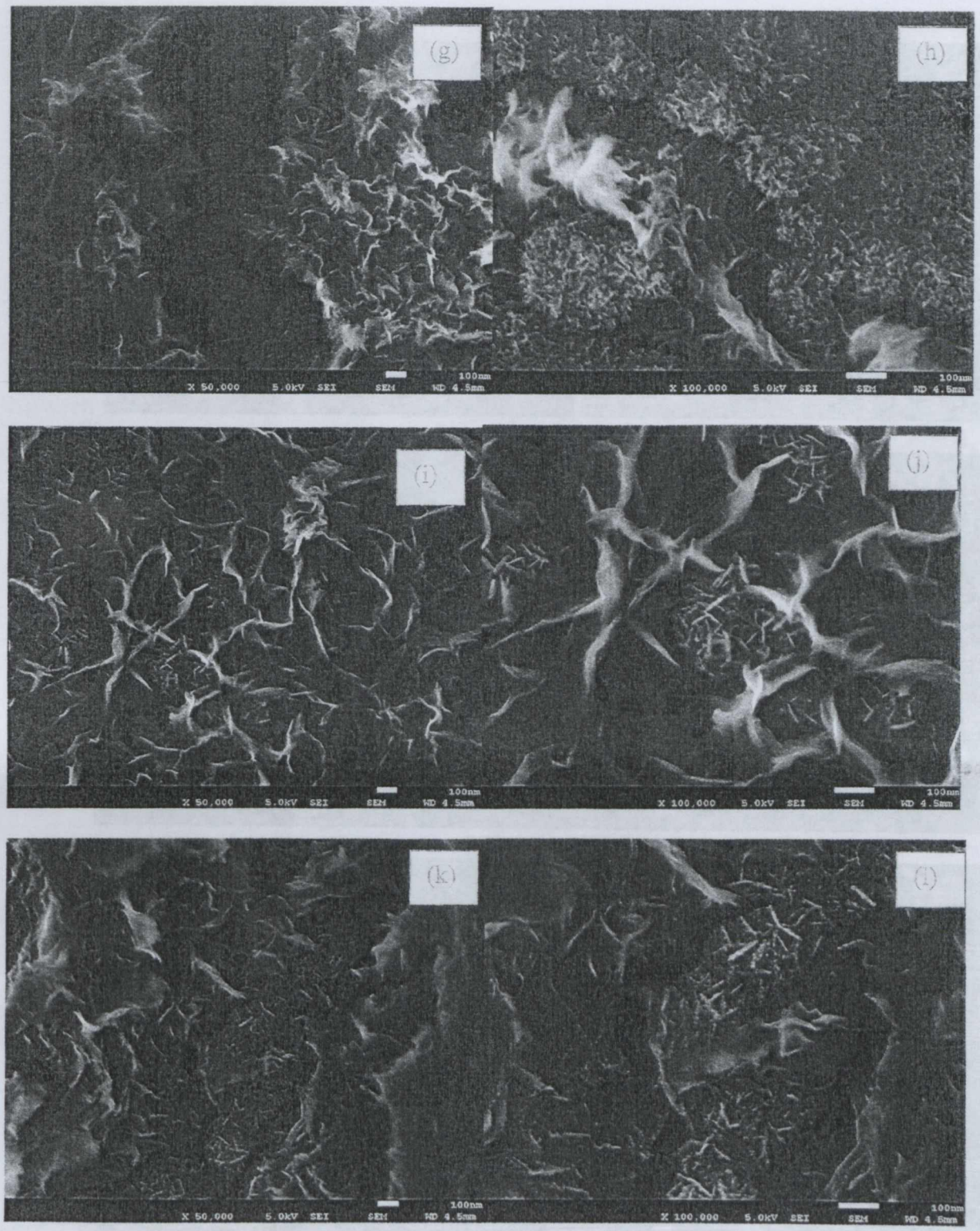

Figure 5: (a, b) before CV test, (c, d)1 mV/s, (e, f) 5 mV/s, (g, h) 10 mV/s, (i, j) 15 mV/s and (k, l) 20 mV/s

Fig. 5(a-b) shows the morphology of the electrode film deposited on stainless steel before any tests. The electrode film's structure consists of randomly distributed curly sheets. Higher magnification shows that the sheets are ultrathin and accessible for electrolyte ions.

After underwent a relatively low scan rate (1 mV s^{-1}) (Fig. 5(a)), the curly sheets became thicker and merged to become nanoparticles with average size of 108-125nm (Fig. 5(c)). The transformation from sheet-like structure to particles is not easily to be seen at low scan rate (1 mV s^{-1}). The particles are hidden beneath the curly sheets since the electrolyte ions can diffuse deeper into the sheet-like structure and react. The particles can be more clearly seen at 5 mV s^{-1} (Fig. 5(e,f)). At higher scan rates (10, 15 and 20 mV s^{-1}), electrolyte ions can only reach to the electrode film surface. Thus, the nanoparticles are burst out onto the surface as seen in Fig. 5(g-l). The red circles in higher magnification (x100K) (Fig. 5(f)) emphasize the connection and relation between sheets and particles. The particles were found to have nanoflakes surface at 15 and 20 mV s^{-1} (Fig. 5(f and h)). This indicates that less reaction was occurred at these two scan rate compared to 1, 5 and 10 mV s^{-1} which leads to less changes on the surface of particles since the as-prepared electrode film displayed sheet form.

3.3 TEM study

In order to examine the microstructure of the electrode film, transmission electron microscopy (TEM) has been carried out. The images of electrode films obtained are shown in Fig. 5.

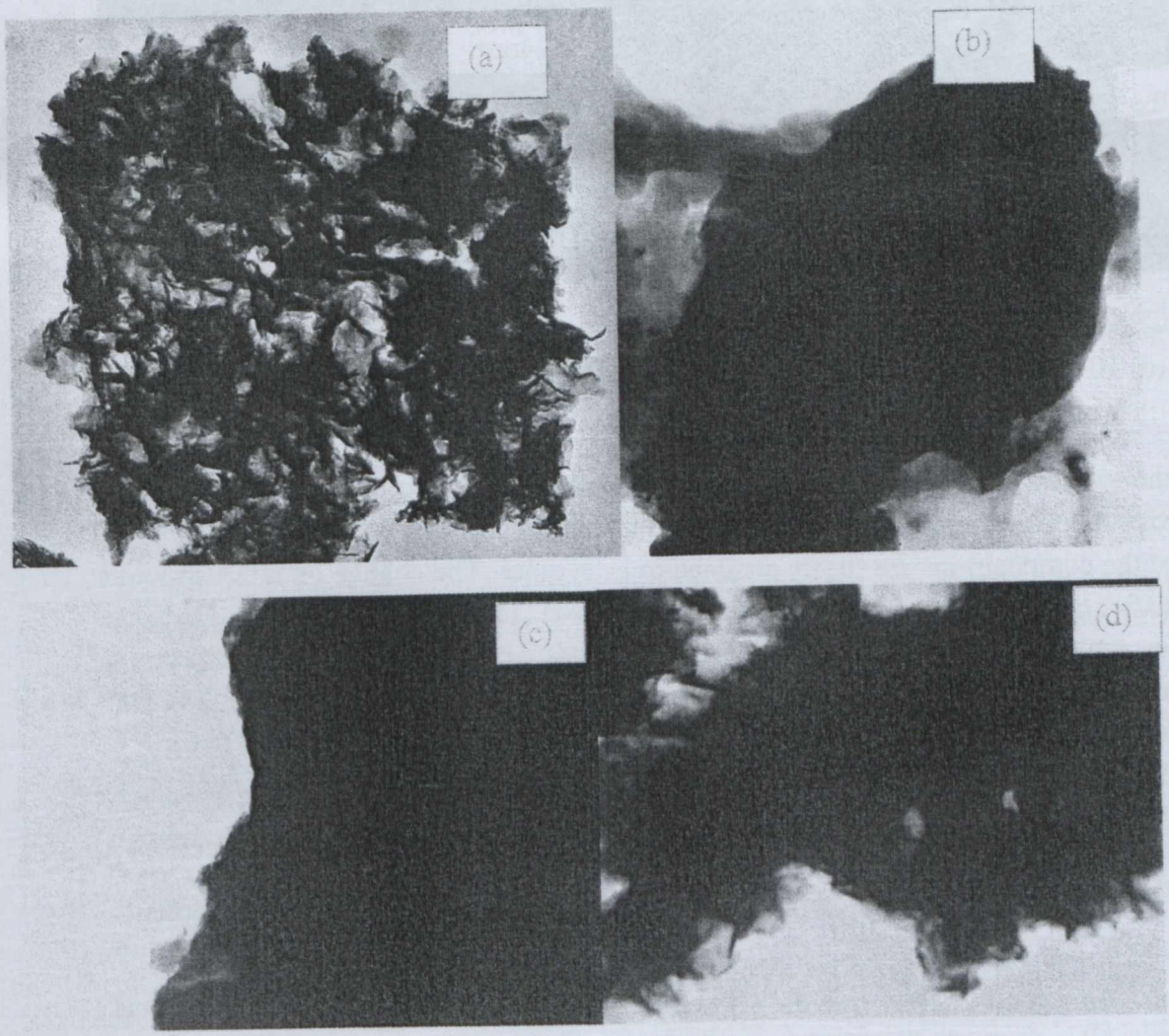

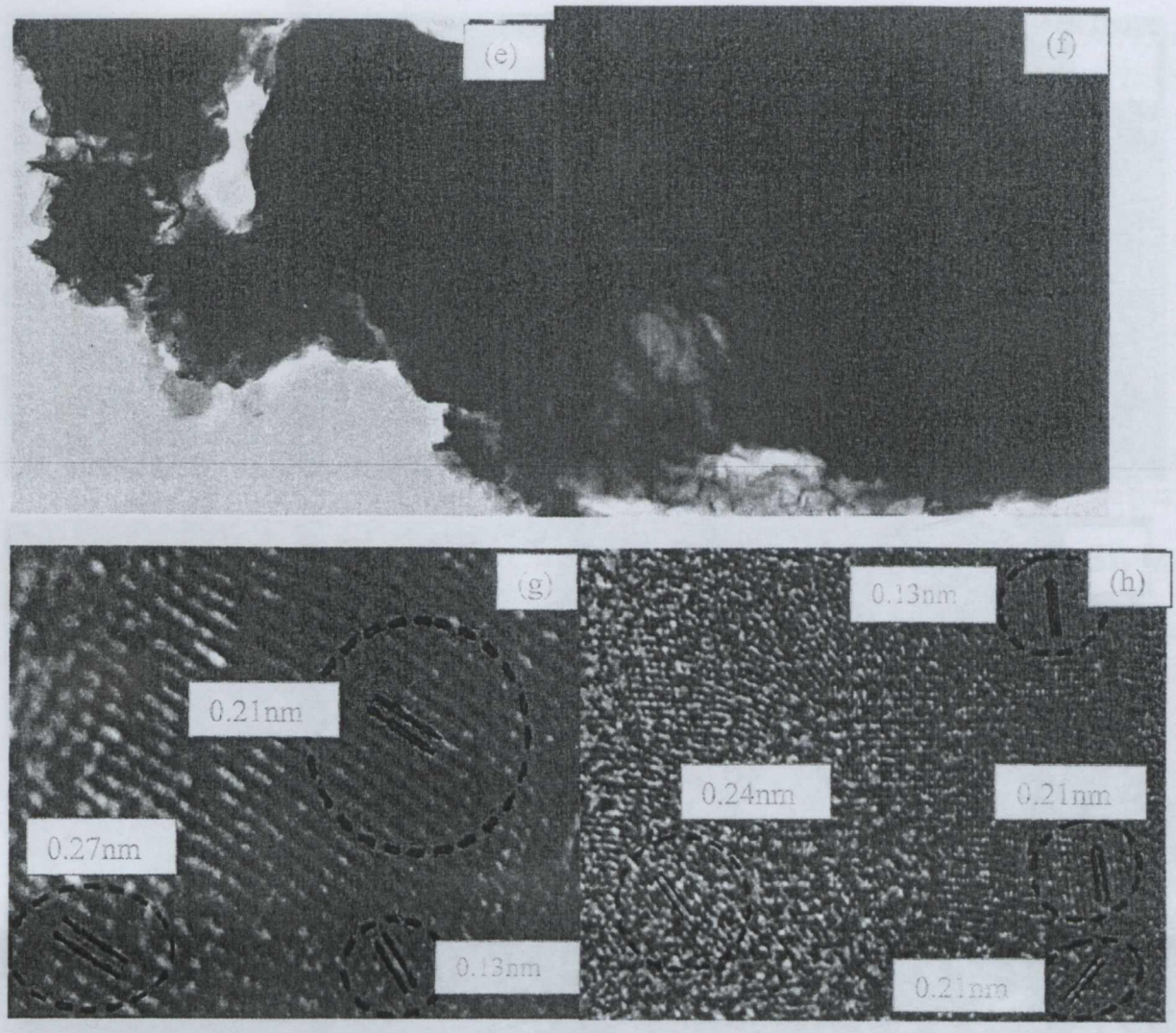

Figure 6: TEM images of (a) as-prepared electrode film, electrode films after (b) 1 mV s^{-1}, (c) 5 mV s^{-1}, (d) 10 mV s^{-1}, (e) 15 mV s^{-1}, (f) 20 mV s^{-1} and (g,h) lattices fringes of as-prepared electrode film.

Fig. 6(a) shows the TEM image of the as-prepared electrode film. It is clear that the sheet-form microstructure is consistent with the FESEM result Fig. 6(a,b). From here we can deduce that the compositions are firmly attached to each other. The change on microstructure is obvious after cyclic voltammetry as shown in Fig. 6(b-f). The dark spot can be regarded to the particles agglomerated. From Fig 6(g,h), lattice fringes with distances of 0.21nm and 0.24nm were found and can be assinged to (200) plane and (111) plane of CoO [12, 24]. On the other hand, 0.27nm lattice spacing can be indexed to (100) plane of α-$Ni(OH)_2$ [11]. Besides, the presence of α-$Ni(OH)_2$ also can be identified through the lattice fringes of 0.13nm which is corresponding to (201) plane [10].

Conclusion

RGO-CoO-$Ni(OH)_2$ composite film has been synthesized successfully using green electrodeposition technique. The effects of scan rate on the morphology and electrochemical performance of the electrode film have been discussed. XRD revealed the amorphousness of

the as-prepared electrode film but no information on the compositions contained. However, the compositions were uncovered after experienced the cyclic voltammetry tests. This may due to the chemically change or dissolution of composite film induced by the interaction between electrolyte ions and electrode film surface. The compositions contained (Co, Ni, O) were supported by EDX study. Besides, XRD patterns of electrode films after different scan rate of cyclic voltammetry confirmed the compositions of electrode films remained the same although the interaction between electrolyte ions and electrode film surface has caused some chemically changes on the electrode film such as insertion of electrolyte ions onto the electrode film surface. Cyclic voltammetry test showed that the electrode film was fully utilized its electroactive sites at 5 mV s^{-1} and achieved specific capacitance of 558 F g^{-1}. Cycle stability test was carried out using cyclic voltammetry method. The electrode film has found to retain around 30% after 1000 cycles. This can be caused by the dissolution of composite film during cycling process. FRA implied the low equivalent series resistance and charge transfer resistance of the as-prepared electrode film. The Randles circuit has been used to fit the experimental data we obtained. The corresponding equivalent circuit consisted of equivalent series resistance (R_s), charge transfer resistance (R_p) and constant phase elements (CPE) which used to replace the capacitive element to explain the non-ideal behaviours of the capacitor. The morphologies after CV tests were changed due to some irreversible reactions with electrolyte ions. TEM displayed the corresponding microstructures of the electrode films to the FESEM images. It exhibited the sheetlike structure of the as-prepared electrode film and the agglomeration of particles after the cyclic voltammetry. Lattice fringes calculated further supported the XRD and EDX results and showed the components contained were CoO and α-$Ni(OH)_2$.

Acknowledgements

The authors acknowledge the University of Malaya for providing financial support through the project HIRG-J21002-73852 and PG010-2013A

References

1. Conway, B.E., *Electrochemical Supercapacitors: Scientific Fundamentals and Technological Applications*. 1999: Springer US. 698.
2. Galizzioli, D., F. Tantardini, and S. Trasatti, *Ruthenium dioxide: a new electrode material. I. Behaviour in acid solutions of inert electrolytes*. Journal of Applied Electrochemistry, 1974. 4(1): p. 57-67.
3. Kuo, S.-L. and N.-L. Wu, *Investigation of Pseudocapacitive Charge-Storage Reaction of MnO2·nH2O Supercapacitors in Aqueous Electrolytes*. Journal of the Electrochemical Society, 2006. 153(7): p. A1317-A1324.
4. Kandalkar, S.G., et al., *Chemical synthesis of cobalt oxide thin film electrode for supercapacitor application*. Synthetic Metals, 2010. 160(11–12): p. 1299-1302.
5. Chen, X.a., et al., *One-pot hydrothermal synthesis of reduced graphene oxide/carbon nanotube/α-Ni(OH)2 composites for high performance electrochemical supercapacitor*. Journal of Power Sources, 2013. 243(0): p. 555-561.
6. An, L., et al., *Exceptional pseudocapacitive properties of hierarchical NiO ultrafine nanowires grown on mesoporous NiO nanosheets*. Journal of Materials Chemistry A, 2014.